EIGENVALUE AND FREQUENCY DOMAIN ANALYSIS OF SMALL-SIGNAL ELECTROMECHANICAL STABILITY PROBLEMS

Nelson Martins, Member IEEE

Centro de Pesquisas de Energia Elétrica – CEPEL
Caixa Postal 2754
Rio de Janeiro, RJ, 21945, Brazil

Leonardo T.G. Lima

MAIN Engenharia S.A.
R. do Ouvidor 121
Rio de Janeiro, RJ, 20040, Brazil

Keywords – Excitation Control, Additional Feedback, Static VAr Compensators, Electromechanical Oscillations, Power System Dynamics, Stability.

Abstract – This paper discusses many aspects related to small-signal electromechanical stability. The major emphasis is on stabilizer signal tuning through eigenvalue and frequency domain techniques. Detailed results and full data are given on the power systems analyzed. Feedback control difficulties associated with badly located zeros are discussed.

1. INTRODUCTION

The analysis and control of electromechanical oscillation damping in power systems [1] has been a subject of large practical interest over the last two decades. This paper has a tutorial nature for addressing various aspects of small-signal electromechanical stability but also reports some new results in the area. Full data and detailed results are here provided for stabilizer tuning examples in single-machine and multimachine systems. This information may prove valuable for engineers willing to validate their small-signal stability software.

Section 2 of this paper contains a brief review of the algorithms presently employed in the linear analysis of the small-signal electromechanical stability of large power systems [2–10].

Section 3 describes tuning procedures for additional stabilizing signals through the use of eigenvalue and frequency response techniques. Stabilizer tuning has been widely described in the technical literature, and [11–15] together with associated references are representative of this work. Section 3 presents extensive results, including a few original ones, regarding the use of different input signals to a stabilizer. The procedure described can be used for tuning stabilizing signals added to generator exciters, static VAr compensators, HVDC systems or to any other component in the system.

The effects of load modelling on small-signal stability are presented in Section 5 in the form of stability regions for a single-machine infinite-bus system supplying a load. Results concerning load modelling effects on a multimachine system are included in Section 6.

The multimachine system analyzed in Section 6 shows stabilization difficulties associated with a complex pair of zeros located on the right-half-plane. This type of problem does not occur on single-machine-infinite-bus systems and requires multimachine eigenvalue and frequency domain methods to be detected, analyzed and solved. The results of Section 6 regarding power system zeros [2,16] are considered to be of particular value. Transfer function residues [1,2] can be effectively used to determine the most adequate locations for placing damping sources in a power system. Results on residue ranking for PSS location are given in Section 6.

The complete data of the test systems studied are given in the appendices so that every result of this paper may be reproduced. These results were obtained by a comprehensive small-signal stability analysis package. Such a package is of high value to the analysis of a range of small-signal stability problems as will be seen in the paper.

The redundancy in the rotor swing state variables of a multimachine matrix was not correctly interpreted in some classical papers on this field. Though this problem may now be well understood, the material of Appendix 5 is of interest.

2. OVERVIEW OF METHODS FOR SMALL SIGNAL STABILITY ANALYSIS

The power system electromechanical stability problem can be represented by a set of differential equations together with a set of algebraic equations, to be solved simultaneously with each other:

$$\begin{aligned} \dot{\underline{x}} &= f(\underline{x}, \underline{z}) \\ \underline{0} &= g(\underline{x}, \underline{z}) \end{aligned} \qquad (2.1)$$

where $\underline{x}$ is the state vector and $\underline{z}$ is a vector of algebraic variables.

Small-signal stability analysis involves the linearization of (2.1) around a system operating point $(\underline{x}_o, \underline{z}_o)$:

$$\begin{bmatrix} \Delta\dot{\underline{x}} \\ \underline{0} \end{bmatrix} = \begin{bmatrix} J_1 & J_2 \\ J_3 & J_4 \end{bmatrix} \begin{bmatrix} \Delta\underline{x} \\ \Delta\underline{z} \end{bmatrix} \qquad (2.2)$$

The power system state matrix can be obtained by eliminating the vector of algebraic variables $\Delta\underline{z}$ in equation (2.2):

$$\Delta\dot{\underline{x}} = (J_1 - J_2 J_4^{-1} J_3)\, \Delta\underline{x} = A\, \Delta\underline{x} \qquad (2.3)$$

The symbol A is used to represent the system state matrix, whose eigenvalues provide information on the singular point stability of the non-linear system.

The symbol Δ signifies an incremental change from a steady-state value and will often be omitted in the remaining part of this paper.

2.1 Traditional Algorithms

For many years, programs have been developed to form explicitly the state space equations:

$$\begin{aligned} \dot{\underline{x}} &= A\,\underline{x} + \underline{b}\,u \\ y &= C\,\underline{x} \end{aligned} \tag{2.4}$$

Full eigensolution of non-sparse matrix A is normally restricted to systems of moderate size (below 500 states) due to the large memory and computation time requirements.

The transfer function F(s) relating the input (u) and output(y) variables is obtained from the Laplace transformation of the equation shown in (2.4):

$$F(s) = C(sI - A)^{-1}\,\underline{b} \tag{2.5}$$

The frequency response analysis of dynamic systems can be performed by replacing the Laplace variable "s" by "$j\omega$" in equation (2.5) and numerically calculating $F(j\omega)$ for discrete values or "$j\omega$" within the frequency range of interest. The use of equation (2.5) becomes prohibitive for large order systems due to excessive computational time and memory requirements.

Transfer function residue calculation [1,2], time response to step disturbance and many other needed functions are all prohibitive for large scale systems using this traditional formulation.

2.2 Algorithms for Large Scale Systems

The basic concept that allows the methods of the previous section to be applied to large scale systems is the use of the "augmented system equations" [3], which is now described.

The basic equation relating state matrix, eigenvalues and eigenvectors is:

$$A\,\underline{u}_i = \lambda_i\,\underline{u}_i \tag{2.6}$$

where λ_i is the i-th eigenvalue and $\underline{u}_i$ its associated eigenvector.

An equation equivalent to (2.6) can be made in terms of the Jacobian matrix shown in (2.2).

$$\begin{bmatrix} J_1 & J_2 \\ J_3 & J_4 \end{bmatrix} \begin{bmatrix} \underline{u}_i \\ \underline{z}_i \end{bmatrix} = \lambda_i \begin{bmatrix} \underline{u}_i \\ \underline{0} \end{bmatrix} \tag{2.7}$$

where $(\underline{u}_i^t\,,\,\underline{z}_i^t)^t$ is the augmented eigenvector of λ_i and is denoted by $\underline{u}_i^a$.

The state space equations of (2.4) can in a similar way be expressed as:

$$\begin{bmatrix} \dot{\underline{x}} \\ \underline{0} \end{bmatrix} = \begin{bmatrix} J_1 & J_2 \\ J_3 & J_4 \end{bmatrix} \begin{bmatrix} \underline{x} \\ \underline{z} \end{bmatrix} + \begin{bmatrix} \underline{b}^a \end{bmatrix} u \tag{2.8}$$

$$y = [C_x \,|\, C_z] \begin{bmatrix} \underline{x} \\ \underline{z} \end{bmatrix} = C^a\,\underline{x}^a$$

where

$\underline{b}^a$ = augmented input vector
C^a = augmented output matrix
$\underline{x}^a$ = augmented state vector

The large advantage of equation (2.8) is that the system Jacobian matrix is highly sparse and allows the use of efficient sparsity-based algorithms. The main algorithms for the solution of small-signal stability problems which make use of the augmented system equations concept are listed below.

One-at-a-time-eigenvalue calculation

1. Inverse Iteration Method [3]
2. PEALS [4]
3. Newton Raphson Method [5]

Simultaneous calculation of a group of relevant eigenvalues

4. Lanczos Method applied to $f(A) = (A + hI)(A-hI)^{-1}$ [6]
5. Simultaneous Iterations applied to $f(A) = (A-qI)^{-1}$ [7]
6. Modified Arnoldi Method applied to $f(A) = (A-qI)^{-1}$ [7]

An interesting review on eigenvalue methods for very large power systems may be found in [8].

Efficient Calculation of:

7. Frequency Response Plots [3]
8. Participation Factors [4,9]
9. Transfer Function Residues, Controllability and Observability Factors [2]
10. Linear Time Response to Step Disturbance [3]
11. External System Equivalent in Terms of Frequency Response Relationships Between Injected Current and Voltages at Boundary Buses [10]
12. Eigenvalue Sensitivities to Controller Parameter Changes [5]

A modern package for the small-signal analysis of power systems should have a good part of the above listed algorithms. The package must also have the possibility of obtaining full eigensolution (for mid-size systems) by explicitly forming the state matrix through Gaussian elimination on the Jacobian (see equation (2.2)). This obviates the need to have a different eigenvalue program to perform full eigensolution.

A production grade software must have ease of data input, flexible user defined controller models capable of sensing any combination of local and remote system variables and good program output. Program efficiency may be slightly sacrificed in favour of the above facilities.

3. STABILIZER DESIGN THROUGH EIGENVALUE AND FREQUENCY RESPONSE METHODS

The stabilizer design techniques will be here discussed in connection with the Study System I described in the next item.

3.1 Study System I

The Study System I is shown schematically in Figure 1 and comprises a synchronous generator connected to an infinite bus through a long line. At the middle of the transmission line there are a capacitor bank and a static VAr compensator.

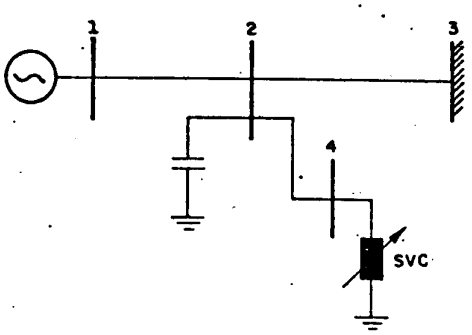

Figure 1. Configuration of Study System I

All system data are given in Appendix 1. The synchronous generator has a 5th order model while the automatic voltage regulator (AVR) has a first-order model. The power system stabilizer (PSS) inputs considered in this paper are rotor speed (ω), terminal power (P_t), bus frequency ($\dot{\theta}$) and apparent line resistance(R).

The block diagram of the static compensator and its stabilizing signal is shown in Figure 2. The input signal to the compensator stabilizer is bus frequency ($\dot{\theta}$) or transit power deviations in a line (P_{ij}).

The system operating point corresponds to a heavy load condition and the angle displacement between the infinite bus and the generator field voltage is 104°. This operating point was chosen to magnify the stabilizing control problem with no consideration given to the transient stability performance of the system. The stabilizing signal loop gains were also made slightly higher than needed, yielding electromechanical mode dampings beyond usual design values.

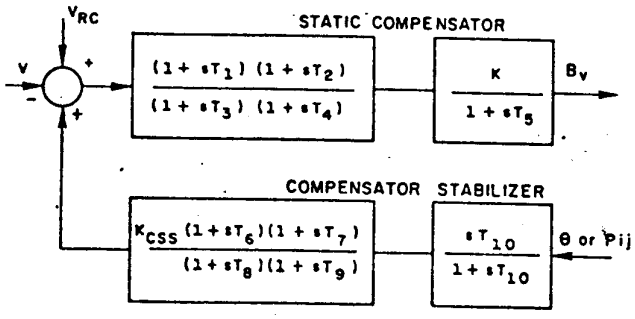

Figure 2. Block Diagram of Static VAr Compensator

3.2 Eigenvalue Results

The static compensator is not absorbing nor generating reactive power for the operating point considered. The eigenvalue analysis for this operating point, considering the presence or absence of different system controllers, clearly shows their effect on the small-signal stability of the system.

Table 1.a shows the eigenvalues for the system with no static VAr compensator (SVC) nor automatic voltage regulator (AVR). The system is of 5th order and suffers from aperiodic instability ($\lambda = +0.196$) due to the lack of synchronizing torques. Including the static compensator model (Table 1c) the system becomes of 8th order and presents a very slow aperiodic instability ($\lambda = +0.002$). This result shows that the SVC significantly increases the generator synchronizing torques.

The system with AVR but without SVC is of 6th order and presents oscillatory instability (see Table 1.b) due to the negative damping introduced by the AVR [11]. Table 1.d lists the eigenvalues for the system having both AVR and SVC. The system is of 9th order and shows oscillatory instability ($\lambda = +0.493 \pm j5.08$). From the eigensolutions shown in tables 1.b and 1.d it can be seen that the SVC partly cancels the negative damping introduced by the AVR. The other results shown in Table 1 will be discussed in the remaining part of this section and are relative to System I having both AVR and SVC and incorporating different stabilizing signals. Note that the complex eigenvalue pair associated with the generator electromechanical oscillation (hunting mode) is bold-faced for easy reference in all eigensolutions shown in Table 1.

Table 1. Eigenvalue Results for System I

(a) no AVR, no SVC	(b) with AVR, no SVC
−35.5	−38.20
−0.399 ± j 4.33	−13.06
+0.196	**+0.883 ± j 4.50**
−2.81	−4.71 ± j 1.39

(c) no AVR, with SVC	(d) with AVR, with SVC
−419.8	−419.8
−35.5	−38.17
−0.184 ± j 5.03	−13.26
−3.74	**+0.493 ± j 5.08**
+0.002	−5.61
−0.982 ± j 0.128	−3.62
	−0.958 ± j 0.172

(e) with PSS_1	(f) with PSS_2
−419.8	−419.8
−32.03 ± j 2.083	−38.18
−6.248 ± j 8.051	−13.19
−0.586 ± j 4.899	−7.329
−5.01	−0.583 ± j 5.257
−3.626	−0.293 ± j 2.033
−0.958 ± j 0.173	−3.728
−0.338	−0.267
	−0.972 ± j 0.154

(g) with PSS_3	(h) with PSS_4
−419.8	−998.7
−39.28	−419.8
−10.22	−70.40
−0.616 ± j5.007	−0.399 ± j15.60
−4.387 ± j2.428	−0.605 ± j4.705
−0.960 ± j0.171	−5.810 ± j0.535
−3.748	−3.626
−0.332	−0.959 ± j0.172
	−0.335

(i) with PSS_5	(j) with CSS_1
−419.8	−1007.
−39.75	−410.
−9.41	−37.17
−0.582 ± j5.171	−14.44
−3.799 ± j3.807	−0.602 ± j4.867
−3.762	−5.204 ± j0.996
−0.956 ± j0.185	−2.637
−0.146	−0.950 ± j0.185
	−0.345

(k) with CSS_2	(ℓ) with CSS_3
−37.1	−394.
+ 0.0340 ± j90.3	−38.18
−16.3	−21.01
−8.76	−16.46
−0.0146 ± i4.94	−1.689 ± j9.930
−5.24	−7.785
−3.63	−0.585 ± j4.831
−0.958 ± 0.172	−3.320 ± j0.771
−0.333	−0.959 ± j0.172
	−0.333

3.3 PSS Design Through the Torque–Angle Loop

System I with AVR and SVC has a pair of unstable eigenvalues, as shown in Table 1.d. This system can be made stable by installing a power system stabilizer (PSS) to the generator AVR. To improve system damping, the PSS must produce a component of electrical torque in phase with rotor speed variations. This basic concept has been extensively used to tune stabilizers [11]. The power system needs to be modelled through the generator torque–angle loop, as shown in Figure 3. This block diagram has been well explained in the technical literature related to synchronizing and damping torques and generator stabilizer tuning (see [11] and associated references).

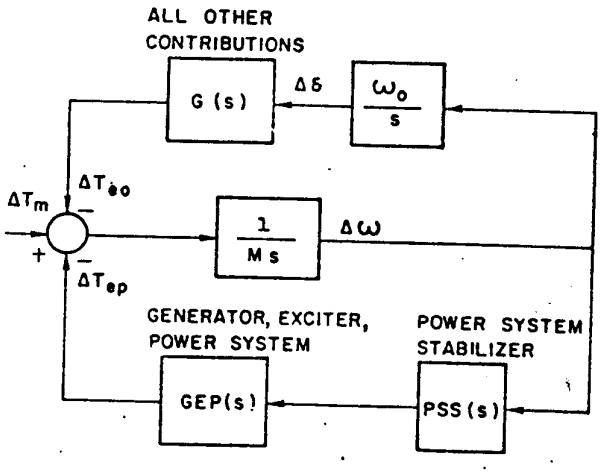

Figure 3. Generator Torque–Angle Loop

In order to provide damping torques through the PSS, it is required that the PSS transfer function compensates for the phase lag of GEP(s) over the range of frequencies of the electromechanical oscillations. Note that for System I the GEP(s) must take into consideration the dynamic effects of the static compensator at bus 4.

The polar plot of GEP(s) is shown in Figure 4, and we see that at the system electromechanical frequency (5.1 rad/s) the phase lag to be compensated by the PSS is around 80°. The PSS parameters must be adequately chosen in order to provide the right compensation, as described in [11] and in Section 3.5.

The authors recognize the merits of the torque–angle loop analysis for PSS tuning, but favour the use of the AVR control loop analysis, which is described in Section 3.5 of this paper.

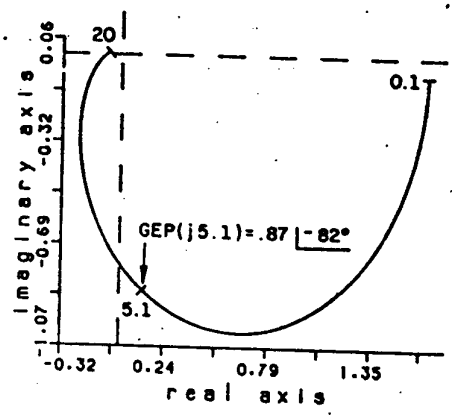

Figure 4. Polar Plot of GEP(s)

3.4 The Nyquist Stability Criterion

This section is very brief since this criterion is well discussed in control theory textbooks. The Nyquist criterion allows the assessment of the closed–loop stability of a feedback system from the knowledge of the open–loop transfer function poles and its frequency response plot. Considering the feedback system shown in Figure 5, the open–loop transfer function (OLTF) is G(s) H(s) and the closed loop transfer function is G(s)/(1+G(s)H(s)).

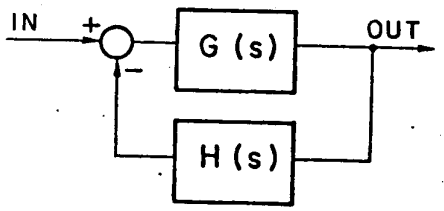

Figure 5. Feedback Control System

The Nyquist criterion stablishes that: $P_c = P_o + N$, where N is the number of clockwise encirclements of the (−1,0) point of the complex plane made by the frequency response plot of the OLTF as the applied frequency varies from $-\infty$ to $+\infty$. P_o and P_c are the number of unstable poles (or eigenvalues) of the open–loop and closed–loop systems respectively. These frequency response plots can be obtained just for positive values of frequencies and in this case they will encircle N/2 times the −1 point of the complex plane. Polar plots or Bode plots can be used to the same effect in this analysis, but the former is preferred by the authors. The terms polar plots and Nyquist plots are used undistinctly in the text.

The design of stabilizing signals applied to generator excitation control systems, static VAr compensators and HVDC links can be carried out using Nyquist plots. In all cases the power system transfer function is G(s), which can be of high order depending on system size, and H(s) is the transfer function of the stabilizing signal to be designed.

Note: The stabilizing signal is normally considered as a positive feedback (see Figures 6, 12 and 15) but the Nyquist stability criterion here applied is for the case of a negative feedback. For this reason, all polar plots shown in the paper were actually multiplied by –1.

3.5 PSS Design Through the AVR Control Loop

Figure 6 shows a block diagram which describes the complete power system dynamics through the AVR control loop. The blocks AVR(s) and PSS(s) correspond to the transfer functions of the automatic voltage regulator and the power system stabilizer respectively. The functions $F_1(s)$ and $F_2(s)$ relate the field voltage with the generator terminal voltage and the variable used as the input to the stabilizer. The dynamic effects of the generator and SVC are considered in $F_1(s)$ and $F_2(s)$, which are 8th order transfer functions. All polar plots shown in this section are for the condition with the voltage feedback loop (block $F_1(s)$ in Figure 6) closed.

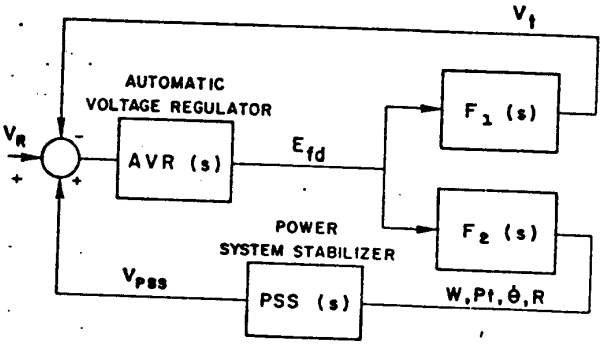

Figure 6. Power System Representation Through the AVR Loop

Speed Input Stabilizer

Figure 7.a shows the polar plot of the transfer function $\Delta\omega(s)/\Delta V_r(s)$, relating rotor speed deviations with AVR reference voltage. The numbers shown near the polar plots are the frequency values of the applied input signal. The system to be stabilized, whose eigensolution is shown in Table 1.d, has a pair of unstable eigenvalues. Therefore $P_o = 2$ and according to the Nyquist stability criterion the polar plot of the OLTF $\Delta V_{pss}(s)/\Delta V_r(s)$ must encircle the –1 point in the counter–clockwise direction ($N = -2$) to ensure stability of the closed loop system ($P_c = 0$).

The initial procedure adopted in stabilizer design is to deduce compensation circuit requirements in terms of gain and phase requirements at the critical frequency 5.1 rad/s. From Figure 7.a it is seen that the PSS blocks should provide around 70 degrees phase advance at 5.1 rad/s. Note that this phase compensation requirement (70°) is about the same as that (80°) identified through the torque–angle loop analysis of Section 3.3. This can be provided by a couple of phase advance units with transfer function

$$\left(\frac{1 + saT}{1 + sT}\right), \qquad \text{where } a > 1.$$

To minimize high frequency gain, which amplifies the signal noise level, the parameter "a" should be as small as possible. The maximum phase–lead angle (ϕ_{max}) obtained with this phase advance unit is given by the expression:

$$\phi_{max} = \sin^{-1}\left(\frac{a - 1}{a + 1}\right)$$

The time constant T determines the frequency ω_{max} at which this maximum phase–lead angle occurs:

$$\omega_{max} = \frac{1}{T\sqrt{a}}$$

The parameter a is chosen by making the maximum phase advance equal to the required phase shift at the frequency of the electromechanical mode. The constant T is chosen so as to make this maximum occur at the frequency of the electromechanical mode.

As the required 70° compensation is provided by two phase advance units (the derivative block $sT_w/(1 + sT_w)$ does not add any significant phase shift at the electromechanical frequency) the value of ϕ_{max} is 35°. For this ϕ_{max} and ω_{max} = 5.1 rad/s we calculate a = 4 and T = 0.098 s. These values are however not critical and deviations from them are quite acceptable. The polar plot for the OLTF $\Delta V_{pss}(s)/\Delta V_r(s)$ with the $PSS_1(s)$ stabilizer is shown in Figure 7.b (this stabilizer has a=4 and T=0.075). Note that the polar plot encircling the –1 point should be approximately symmetrical with respect to the real axis to yield good phase margin. Figure 7.b shows that once the correct phase shift is achieved, the gain requirement of the stabilizer is not too critical with regard to stability margins. This fact is further explained in the following lines.

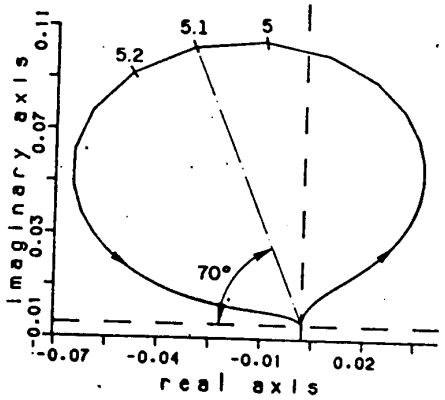

Figure 7.a. Polar Plot of $\Delta\omega(s)/\Delta V_r(s)$

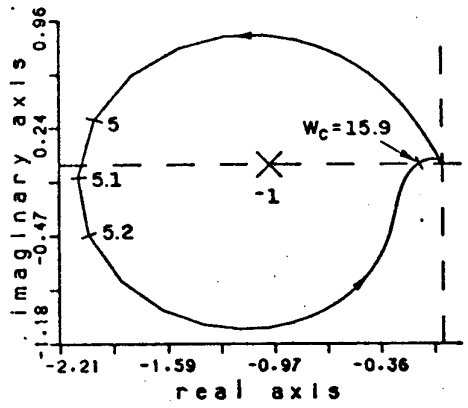

Figure 7.b. Polar Plot of $\Delta V_{pss}(s)/\Delta V_r(s)$ for $PSS_1(s)$ derived from rotor speed (phase–lead)

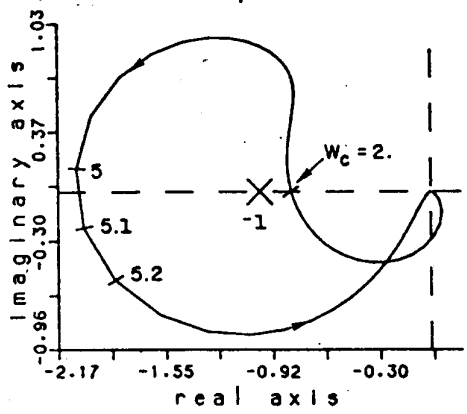

Figure 7.c. Polar Plot of $\Delta V_{pss}(s)/\Delta V_r(s)$for $PSS_2(s)$ derived from rotor speed (phase–lag)

The root locus for the two critical pair of poles in the system is pictured in Figure 8. Only the upper–half of the plot is shown; the lower–half is a mirror image of the upper–half. The root locus plot shows that system stability is maintained for $3.3 < K_{pss} < 50$. A value larger than 50 turns the exciter mode unstable while a value smaller than 3.3 turns unstable the electromechanical mode. This fact can be directly seen from the polar plot of Figure 7.b, since it varies linearly with the PSS gain. The polar plot cuts the negative real axis at points –2.12 and –0.14 for applied frequencies 5.1 and 15.9 rad/s respectively. System stability is maintained if the PSS gain is within limit values given by the ratios: 7/2.12 and 7/0.14, where 7 is the gain value used to obtain the polar plot. This polar plot result indicates that the root–locus crosses the $j\omega$–axis at points j 5.1 and j 15.9 for gain values 3.3 and 50 respectively. The frequencies 5.1 and 15.9 rad/s are known in control theory terminology as phase–crossover frequencies. The symbol w_c is used in the polar plots of this paper to denote a phase–crossover frequency.

The eigensolution for System I with the $PSS_1(s)$ stabilizer is shown in Table 1.e.

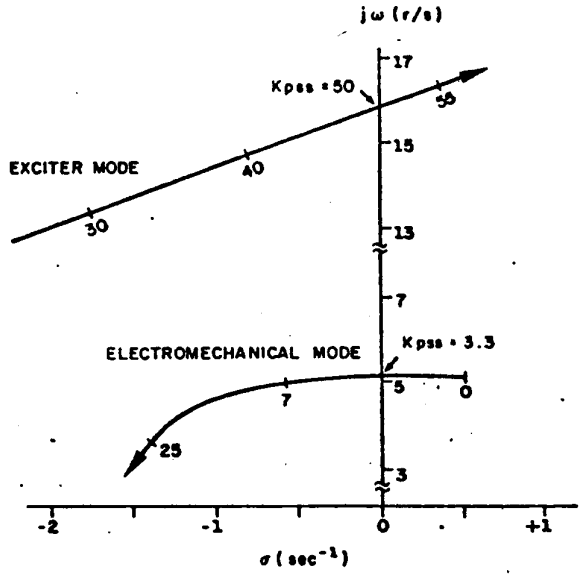

Figure 8. Root Locus for $PSS_1(s)$ Stabilizer

Note, from Figure 7.a, that the system can also be stabilized by phase retarding the speed signal by approximately 110° at about 5.1 rad/s and subtracting it from the voltage reference signal (V_r). This requirement is fulfilled by the phase–lag transfer function $PSS_2(s)$ shown in the Appendix. The Nyquist plot for the OLTF $\Delta V_{pss}(s)/\Delta V_r(s)$ with the $PSS_2(s)$ transfer function is pictured in Figure 7.c, where it is seen that the range of gain values for system stability is $56.8 < K_{pss} < 143$. Note that the ratio between these two gain values (143/56.8) is considerably smaller than that obtained with the $PSS_1(s)$ stabilizer (50/3.3). The eigensolution for System I with the $PSS_2(s)$ stabilizer is shown in Table 1.f.

It is interesting to note that by phase retarding the speed signal, the system shows a curious change in its behaviour. With the rise of the PSS gain the system will become unstable and show growing oscillations at a frequency lower than that of the electromechanical mode (the higher frequency Exciter Mode disappears). When the gain of the $PSS_2(s)$ stabilizer is set to –150, the dominant system eigenvalues are $\lambda = +0.0637 \pm j\,1.969$ and $\lambda = -0.815 \pm 5.475$.

Phase retarding the speed signal is not recommended and these results are only included to show the usefulness of the frequency response technique. In large system models, a phase retarded speed signal usually leads to a low frequency unstable mode for practical values of loop gain.

Power Input Stabilizer

Generator accelerating power has an inherent 90° phase advance with respect to rotor speed, and presently is considered the best signal choice for stabilization through the excitation control system. This signal can not be directly measured, but can be synthetized as shown in [17].In System I, due to the absence of mechanical power variations and stator resistive losses, generator terminal power equals accelerating power except for a sign change. An analysis of the polar plot of function $\Delta P_t(s)/\Delta V_r(s)$ (see Appendix 4) indicates that a finely tuned PSS needs a small phase lag at 5.1 rad/s. The polar plot for the OLTF $\Delta V_{pss}(s)/\Delta V_r(s)$, relative to a stabilizer sensitive to generator terminal power ($PSS_3(s)$ of Appendix I), is pictured in Figure 9 where the range of gain values for system stability is $0.35 < K_{pss} < 17.5$. Note that the ratio of these two gain values (17.5/0.35) is considerably larger than that obtained with the $PSS_1(s)$ stabilizer. The eigensolution for System I with the $PSS_3(s)$ stabilizer is given in Table 1.g.

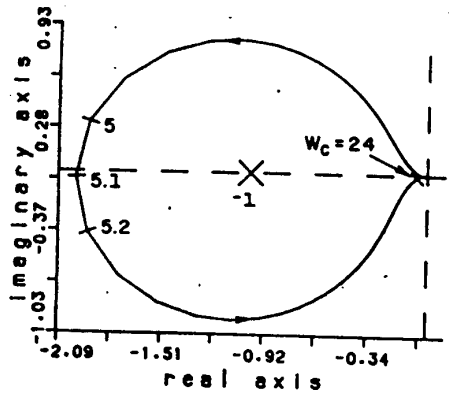

Figure 9. Plot of $\Delta V_{pss}(s)/\Delta V_t(s)$ for $PSS_3(s)$ sensitive to generator terminal power.

Frequency Input Stabilizer

Let us now consider the generator terminal bus frequency as the stabilizer input signal. The polar plot for the OLTF $\Delta V_{pss}(s)/\Delta V_t(s)$, when considering the $PSS_4(s)$ stabilizer, is shown in Figure 10. The range of stabilizer gain values for system stability is $4.16 < K_{pss} < 10.96$. Note that the ratio between these two gain values (10.96/4.16) is considerably smaller than that obtained with the $PSS_1(s)$ stabilizer. The eigensolution for System I with the $PSS_4(s)$ stabilizer is shown in Table 1.h. It is seen that, for the same level of damping for the electromechanical mode, the exciter mode ($\lambda = -0.399 \pm j\ 15.60$) is already lightly damped. These results indicate that the generator bus frequency signal yields reduced gain margins when compared to the generator rotor speed signal. Note that the rotor speed signal can be approximately obtained from measurement of frequency of a synthetic voltage simulating the q-axis voltage ($E_q = V_t + j\,I\,X_q$) as described in [17].

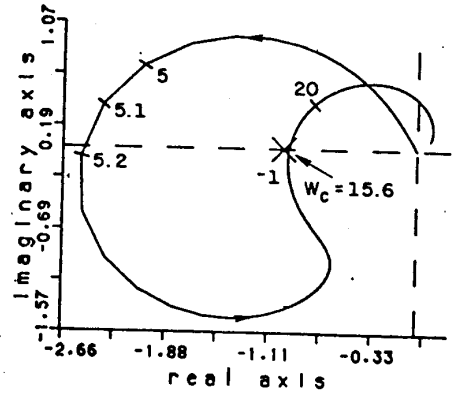

Figure 10. Plot of $\Delta V_{pss}(s)/\Delta V_t(s)$ for $PSS_4(s)$ sensitive to generator bus frequency

We found that the frequency of the synthetic voltage E_q had a slightly better performance than the rotor speed signal as regards stabilizer gain margins. The phase compensation requirements of these two signals were equal for practical purposes. The results obtained therefore indicate that the frequency of voltage E_q is considerably superior to the terminal bus frequency as a stabilizer input signal.

Line Resistance Input Stabilizer

Another stabilizer input signal considered in the literature is the transmission line apparent resistance: $R = P/I^2$. The polar plot of $V_{pss}(s)/V_t(s)$ for the $PSS_5(s)$ stabilizer, which is derived from a line apparent resistance signal, is pictured in Figure 11 and shows that system stability occurs when $0.75 < K_{pss} < 19.5$. The eigensolution for System I with the $PSS_5(s)$ stabilizer is shown in Table 1.i.

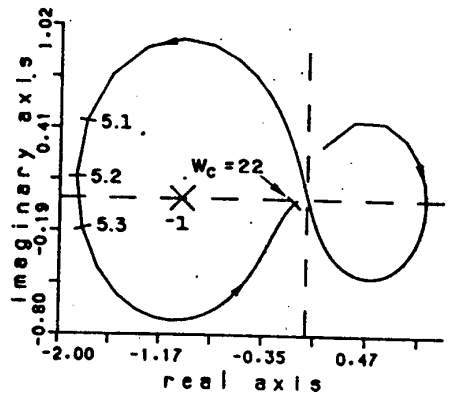

Figure 11. Plot of $\Delta V_{pss}(s)/\Delta V_t(s)$ for $PSS_5(s)$ derived from apparent line resistance

Further Comments

It is convenient to mention the case in which the OLTF has a pair of undamped but stable poles. A correctly tuned PSS in this case, aimed at damping this pole pair, should make the polar plot encircle the (+1,0) point of the complex plane. This polar plot should also be approximately symmetric with respect to the real axis of the complex plane to characterize a good PSS design.

Note that PSS design could also be carried out by considering a different open-loop transfer function (OLTF) in the block-diagram of Figure 3. The OLTF adopted in [12] is AVR(s) $F_1(s)$ + AVR(s) $F_2(s)$ PSS(s), whose polar plot varies linearly with the AVR gain rather than with the PSS gain. The poles for this OLTF are the system eigenvalues when the AVR gain is set to zero.

We conclude by mentioning a large advantage of the AVR-control-loop over the torque-angle-loop analysis: the former can be directly verified (or conducted) through frequency response measurements at the plant [11].

3.6 Stabilizing Signal to the Static Compensator

Stabilizing signals applied to static compensators can effectively damp electromechanical oscillations. Frequency response methods can be used for the design of this stabilizing signal as shown in this section. Figure 12 shows a block diagram which describes the complete power system dynamics through the static compensator control loop. The blocks SVC(s) and CSS(s) denote the transfer functions of the static compensator and its stabilizing signal respectively. The blocks $F_3(s)$ and $F_4(s)$ relate the compensator shunt admittance (B_v) with the deviations in the regulated bus voltage (V) and the system variable used as the input to the stabilizer.

Two stabilizer inputs are here considered: the frequency deviations (θ) at bus 2 and the transit power deviations in the transmission line between buses 2 and 3 ($P_{2\text{-}3}$). All polar plots shown here are for the condition with the voltage feedback loop (block $F_3(s)$ of Figure 12) closed.

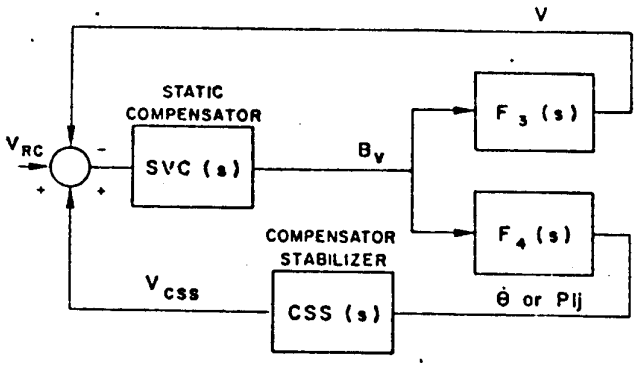

Figure 12. Power System Representation through the SVC Loop

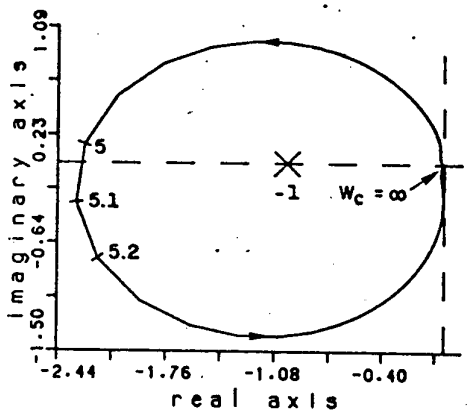

Figure 13. Polar Plot of $\Delta V_{css}(s)/\Delta V_{rc}(s)$ for Stabilizer $CSS_1(s)$

Frequency Input Stabilizer

The open-loop transfer function $\Delta V_{css}(s)/\Delta V_{rc}(s)$ has two unstable poles and therefore its polar plot must encircle the -1 point to ensure closed-loop system stability. The symbol V_{rc} denotes the static compensator reference voltage. Figure 13 shows the plot of $\Delta V_{css}(s)/\Delta V_{rc}(s)$ for stabilizer $CSS_1(s)$ which is sensitive to bus frequency deviations. This plot shows that system stability is obtained for $64.6 < K_{css} < \infty$, where K_{css} is the gain of the compensator stabilizing signal. The eigensolution for System I with the $CSS_1(s)$ stabilizer is shown in Table 1.j.

Line Power Input Stabilizer

The plot of $\Delta P_{2\text{-}3}(s)/\Delta V_{rc}(s)$, where $\Delta P_{2\text{-}3}$ denotes the transit power deviations in the line between buses 2 and 3, is shown in Figure 14.a. The magnitude of this transfer function decays slowly as the applied frequency is increased and still is relatively large for frequencies around 200 rad/s. This fact indicates that stabilizer design will now be of greater complexity than in the previous case. An explanation to this fact can be given by looking at Figure 2 and noting that at high frequencies the following approximation holds:

$$\frac{\Delta B_v(s)}{\Delta P_{2\text{-}3}(s)} = K_{css}\,\frac{T_1\,T_2\,T_6\,T_7}{T_3\,T_4\,T_8\,T_9}\,\frac{K}{(1+s\,T_5)}$$

This transfer function has high gain and low attenuation at high frequencies. The electrical network is modelled by algebraic equations and therefore a component of the transit power $P_{2\text{-}3}$ instantaneously follows any change in the variable shunt admittance B_v. Accordingly, the transfer function $\Delta P_{2\text{-}3}(s)/\Delta V_{rc}(s)$ also shows high gain and low attenuation at high frequencies. This was not observed for $\Delta\theta(s)/\Delta V_{rc}(s)$, since the bus frequency variations are determined by the generator rotor oscillations, which rapidly decay with increasing values of applied frequency due to rotor mechanical inertia.

Figure 14.b shows the polar plot of $\Delta V_{css}(s)/\Delta V_{rc}(s)$ for a stabilizer function $CSS_2(s)$. The stabilizer transfer function provides the right phase compensation at the critical frequency 5.1 rad/s but fails badly at high frequencies. The system eigenvalues are shown in Table 1.k where the electromechanical oscillation mode ($\lambda = -0.0146 \pm j\,4.94$) is not sufficiently damped while a high frequency mode ($\lambda = +0.034 \pm j\,90.3$) is already unstable. The power system model used here is only correct for frequencies up to a few Hertz and the high frequency mode here calculated is therefore largely in error. This result, though approximate, is of interest since it identifies a problem associated with the use of line transit power deviations as a stabilizer signal.

Figure 14.c shows the polar plot of $\Delta V_{css}(s)/\Delta V_{rc}(s)$ for a stabilizer function $CSS_3(s)$ which provides the attenuation needed at high frequencies. The phase advance needed at 5 rad/s is provided by two phase-lead blocks. The two phase-lag blocks reduce the stabilizer gain at higher frequencies, eliminating the instability observed with the $CSS_2(s)$ transfer function. The eigensolution for System I with the $CSS_3(s)$ stabilizer is shown in Table 1.ℓ.

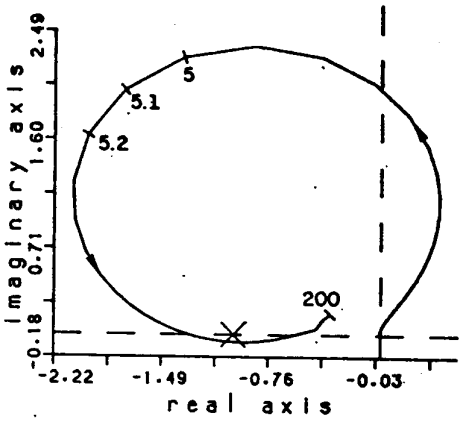

Figure 14.a. Plot of $\Delta P_{2\text{-}3}(s)/\Delta V_{rc}(s)$ (Transit Power Deviations at Line 2-3)

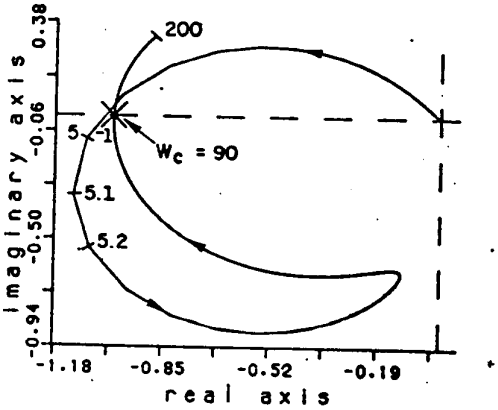

Figure 14.b. Plot of $\Delta V_{css}(s)/\Delta V_{rc}(s)$ for $CSS_2(s)$ Sensitive to $\Delta P_{2\text{-}3}$

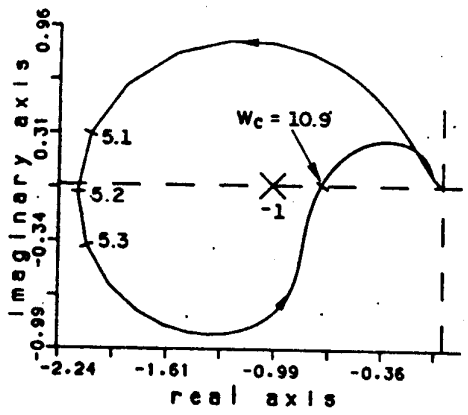

Figure 14.c. Plot of $\Delta V_{css}(s)/\Delta V_{rc}(s)$ for $CSS_3(s)$ Sensitive to ΔP_{2-3}

4. COMMENTS ON HVDC LINK MODULATION FOR ELECTROMECHANICAL DAMPING

HVDC systems have been increasingly used in many parts of the world for bulk power transmission and other applications. They have very fast response and a large potential for damping electromechanical oscillations through DC power modulation.

Figure 15 shows a block diagram which describes the complete power system dynamics through the HVDC converter control loop.

This block diagram is similar to the ones shown in Figures 6 and 12 and can also be used for the frequency response design of stabilizing signals added to the HVDC current controller.

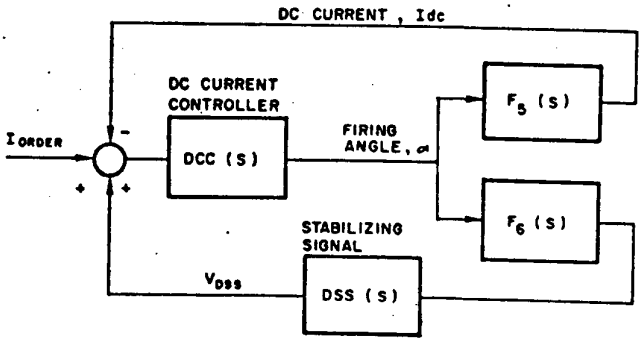

Figure 15. Power System Representation Through the HVDC Converter Control Loop

The blocks DCC(s) and DSS(s) correspond to the transfer functions of the HVDC link current controller and the additional stabilizing signal respectively. The functions $F_5(s)$ and $F_6(s)$ relate the rectifier firing angle with the DC line current and the AC system variable (bus frequency, transit power in a line, etc.) to be fedback through the stabilizing signal respectively.

The analysis of an AC/DC system, involving the design of HVDC link stabilizers through eigenvalue and frequency response methods, will be the subject of a separate publication.

5. LOAD MODELLING EFFECTS ON SMALL-SIGNAL STABILITY

The impact of load modelling on small-signal stability can be more readily appreciated on a single-machine infinite-bus system. Figure 16 depicts the power system studied whose data can be found in Appendix 3. The generator is represented by a 5-th order model, while the fast acting excitation control system and the induction motor load have first and third order models, respectively. The system load, located near the generator, remains with fixed magnitude throughout the study, independent of its dynamic characteristics.

A convenient way of describing small-signal stability limits of a generator connected to an infinite system through a tie line is by expressing the stability regions in terms of the power P + jQ delivered by this generator. These regions are here presented in the P–Q plane with the generator bus voltage held at a constant magnitude [18]. All the changes in P and Q are made by varying conveniently the magnitude and angle of the infinite bus voltage. The P–Q plots of Figure 17 determine the regions to the left of which the system will present oscillatory modes with a damping ratio ξ greater than 0.03, where $\xi = -R/(R^2 + M^2)^{0.5}$ and $\lambda = R \pm jM$. In order to obtain the curves of Figure 17 a few hundred operating conditions were investigated with the use of an eigenvalue program. Figure 17 shows P–Q plots when the active part of the system load is modelled as constant impedance (Z), constant current (I) and constant power (P). Figure 17 also shows P–Q plots for an induction motor load whose value of inertia (H) is seen to have a large impact on the small-signal stability of the system studied. The two plots shown correspond to the same motor parameters except for the inertia constant (H) whose values are 0.5 and 5 seconds.

The curves of Figure 17 also show the large improvement in system damping obtained with the installation of a fixed parameter PSS over the full range of operating conditions and for the different load characteristics.

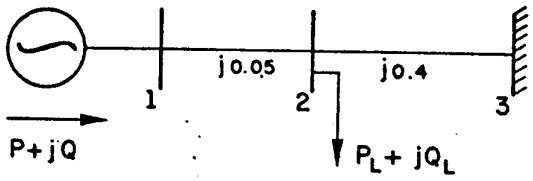

Figure 16. System Used to Obtain P–Q Stability Plot

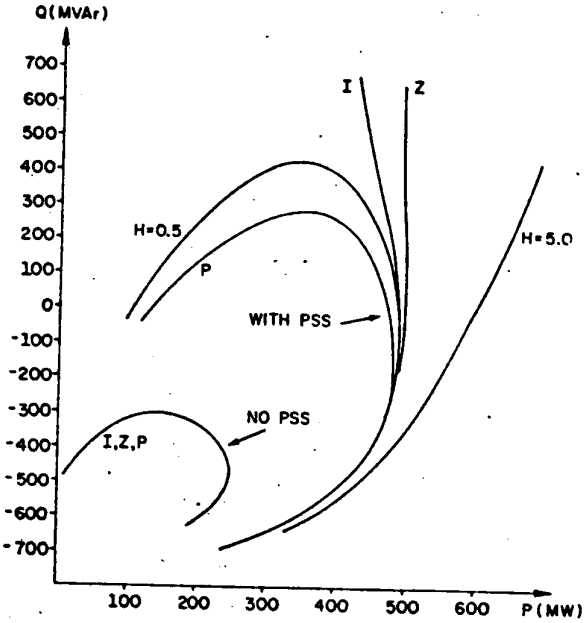

Figure 17. Regions in the P–Q Plane with $\xi > 0.03$

6. STUDY SYSTEM II

The location of the zeros of the OLTF of a feedback system is closely related to the ease with which the system is controlled. If the zeros are so located in the complex plane such that the root locus branches ending on them lie on the right-half-plane (or

close to the imaginary axis) for gains in the range of interest for the closed loop system then they are not suitably located. This fact will be clearly seen in the analysis of Study System II.

The Study System II, pictured in Figure 18, is a slightly modified 7-bus equivalent of the model used in the initial planning studies of the Itaipu generation and AC transmission complex. The Itaipu generator is connected to the Southeast Region (represented by a static load together with a large synchronous motor) through a series compensated 765 kV line. An intermediate 765 kV bus is connected to a 500 kV transmission ring containing three other hydro stations: S. Santiago, S. Segredo and Foz do Areia. The AVR models used in the original system were disregarded in favour of a simpler first-order model which is common to all machines. All loads are of the constant-impedance type. The operating point considered is derived from a heavy load condition of the original system, but the transmitted power in the 765 kV line was raised by an additional 10 percent.

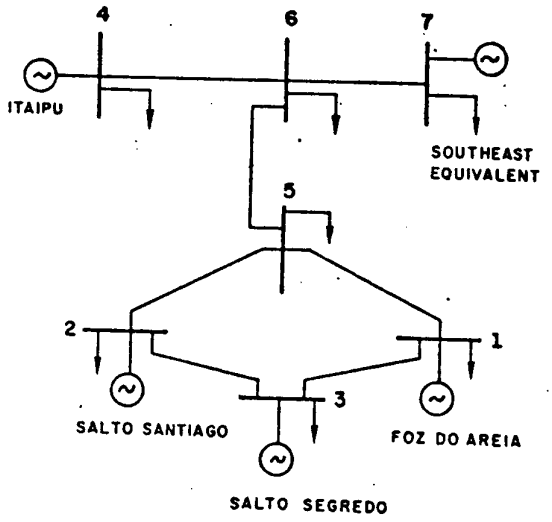

Figure 18. Configuration of Study System II

6.1 Eigenvalue and Frequency Domain Analysis

System II shows a pair of unstable eigenvalues ($\lambda = +0.646 \pm j\ 5.391$) at the operating point investigated. The task we pose ourselves is to damp this unstable mode through the installation of stabilizers to the system generators. The existing stabilizing action on the generators of the Southeast Region, could be approximately represented by a PSS added to the equivalent synchronous-motor, but this effect will not be considered.

The obvious candidate for PSS installation is the Itaipu generator. PSS tuning for the Itaipu generator through the technique previously described requires obtaining the polar plot of the transfer function $\Delta\omega(s)/\Delta V_r(s)$, considering the dynamics of the entire multimachine system. From this plot, shown in Figure 19.a, it is seen to be impossible to stabilize the system just with a stabilizer at Itaipu. This is confirmed by the plot of $\Delta P_t(s)/\Delta V_r(s)$, shown in Figure 19.b, which also cannot be compensated to yield an anti-clockwise encirclement of the -1 point. The polar plot of GEP(s) for the Itaipu generator, pictured at Figure 20.a, indicates that a tuned PSS (though unable to stabilize the system) should provide a 104° phase advance at the critical frequency 5.4 rad/s.

Figure 20.a was obtained when considering the full system dynamics. A leading North-American utility suggests a very simple procedure for stabilizer tuning based on the plot of the GEP(s) for the generator analyzed with nearby generators modelled as negative impedances and remote ones as infinite buses [15]. This corresponds to a single-machine infinite-bus model for the system, in which the equivalent impedance to the infinite-bus is different from the Thevenin's value. Figure 20.b shows the GEP (s) plot obtained according to the method of [15]. Note that it has about the same phase angle (104°) as the plot of Figure 20.a at the electromechanical mode frequency.

The root locus plot of Figure 21 shows the movement of the Itaipu exciter mode and of the two main electromechanical mode poles as the PSS gain of Itaipu is varied. This plot is obtained when considering $PSS_7(s)$ as the transfer function of the Itaipu stabilizer. Note that the unstable electromechanical mode cannot be stabilized by increasing the PSS gain since the associated pole pair is attracted by a complex pair of zeros placed very slightly on the right-half-plane ($z = +0.049 \pm j\ 5.908$). The use of generator terminal power as the input signal to the stabilizer yields a similar root locus since the transfer function $\Delta P_t(s)/\Delta V_r(s)$ has the very same pair of zeros. This happens because $\Delta P_t(s) = -2Hs\ \Delta\omega(s)$ in the absence of mechanical power variations and stator resistive losses.

The use of line apparent resistance as the stabilizer input has in some instances [18] eliminated existing OLTF right-half-plane zeros. This does not happen with System II whose transfer function $\Delta R(s)/\Delta V_r(s)$, R being the line resistance measured at the Itaipu generator terminals, shows a pair of zeros: $z = +0.249 \pm j\ 6.404$.

It is interesting to note that by adding stabilizers to the S. Santiago, S. Segredo and Foz do Areia generators, the unstable mode remains almost unchanged. When the $PSS_6(s)$ stabilizer is simultaneously added to these three generators the unstable eigenvalue pair is: $\lambda = +0.656 \pm j\ 5.379$. If the PSS gains of these three generators are simultaneously raised to infinity, this unstable pole is slightly altered to: $\lambda = +0.658 \pm j\ 5.371$. This unstable mode is therefore not controllable by these three generators.

Consider now the tuning of the Itaipu stabilizer in the presence of stabilizers $PSS_6(s)$ in the other three generators. The polar plot of $\Delta\omega(s)/\Delta V_r(s)$ for the Itaipu generator, shown at Figure 22.a, indicates the system can now be stabilized and that a 100° phase advance is needed at about 5.4 rad/s. The polar plot of $\Delta V_{pss}(s)/\Delta V_r(s)$ for the $PSS_7(s)$ stabilizer is shown in Figure 22.b and informs that system stability is maintained when $25.9 > K_{pss} > 6$. Eigenvalue analysis shows that the least damped eigenvalues are $\lambda = -0.333 \pm j\ 5.206$ and $\lambda = -1.381 \pm j\ 12.21$ for $K_{pss} = 16$. It is evident that the troublesome pair of complex zeros has disappeared from the $\frac{\Delta\omega(s)}{\Delta V_r(s)}$ transfer function of the Itaipu generator. This fact shows the complexity of the power system stabilization problem: stabilizers may be needed in some generators not for being able to damp system poles but for moving away troublesome zeros and making other PSS locations more effective is damping oscillations.

Note also that improper location of transfer function zeros does not necessarily mean they need to be on the right-half-plane. A 10 percent reduction on the power interchange between the Itaipu and the Southeast Equivalent machines causes the troublesome pair of zeros to move slightly into the left-half-plane, but the system continues to present basically the same stabilization problem.

The troublesome eigenvalue and zero pairs of the Itaipu generator transfer function become $\lambda = +0.667 \pm j\ 5.315$ and $z = -0.242 \pm j\ 5.66$ when AVR action is neglected on the three generators of the 500 kV ring. A single PSS located at the Itaipu generator can now stabilize the system through modulation of the impedance loads of the 500 kV ring. Note that the maximum damping achieved for the electromechanical eigenvalue is about 4% since it will coincide with $z = -0.242 \pm j\ 5.66$ for infinite gain at the Itaipu stabilizer.

6.2 Transfer Function Residues

Transfer function residues [1] or controllability factors [13] can be effectively used for determining the most suitable location for placing damping sources in large power systems [2]. Transfer

function residues have also been used in stabilizer tuning [1].

This section provides results on transfer function residues of System II. The reader should refer to [1,2] for theoretical aspects and results for large practical systems.

The residues for the $\frac{\Delta P_t(s)}{\Delta V_r(s)}$ transfer function of the System II generators are given in Table 2 for the unstable eigenvalue.

GENERATORS	RESIDUE	
	Magnitude	Phase
Itaipu	6.70	31.6°
Equivalent	5.55	165.°
F. Areia	0.044	162.°
S. Segredo	0.042	160.°
S. Santiago	0.027	144.°

Table 2. Residues of $\Delta P_t^k(s)/\Delta V_r^k(s)$ for $\lambda = +0.646 + j\,5.391$ (k = 1,.2,..5)

The generator ranking for PSS location is based on residue magnitude. The Itaipu and Southeast Equivalent Machines are seen in Table 2 to have large residues and therefore should be effective in damping the troublesome eigenvalue when equipped with stabilizers. The phase of the residues provide approximate information on the stabilizer compensation requirements[1]. Note that the other three generators have a relatively small residue magnitude, suggesting the existence of transfer functions zeros in the vicinity of the unstable eigenvalue. This information confirms the eigenvalue results of Section 6.1: these three generators are unable to shift the unstable eigenvalue through excitation control.

In the absence of mechanical power variations, which is the case in this study, there is a fixed relation between the residues of the $\frac{\Delta P_t(s)}{\Delta V_r(s)}$ and $\frac{\Delta \omega(s)}{\Delta V_r(s)}$ transfer functions of a given generator[2]:

$$R_i^{P_t} = -(2\,H\,\lambda_i + D)R_i^{\omega}$$

The superscripts ω and P_t denote residues associated with the output variables ω and P_t respectively. The symbols H and D represent the inertia and the mechanical damping constants of the generator.

6.3 Load Modelling Effects on System II

The effect of the voltage sensitivity of the loads on the critical eigenvalue pair of System II is shown in Table 3 for three values of gain for the Itaipu stabilizer. Apart from the Itaipu $PSS_7(s)$ stabilizer the three other generators are equipped with the $PSS_6(s)$ stabilizer. The loads at all buses in the system were modelled as constant impedances or had their active parts represented as constant current or constant powers.

Table 3 shows that, for $K_{pss} = 0$ and $K_{pss} = 8$, the electromechanical oscillation damping problem is worsened when changing the load model from constant impedance to constant current or constant power. The linear responses of Figure 23.a and 23.b confirm the eigenvalue results showing stable oscillations for constant impedance and unstable ones for constant power loads. The disturbance applied was a pulse in the reference voltage of the Itaipu AVR, with 30 ms duration and a 0.01 p.u. magnitude.

Note that for $K_{pss} = 16$, the electromechanical eigenvalue obtained with the constant power load model has higher damping than that obtained with the other two load models. This result shows that the accepted idea that constant power loads are detrimental to stabilizer damping action is not valid in all cases.

The linear response results of Figure 23.c and 23.d are for $K_{pss} = 16$ at the Itaipu stabilizer. Note that the large difference in eigenvalue damping between cases with constant Z and constant P load models is not readily detected in the step response results due to the contributions of other system modes and the different location of the transfer function zeros.

LOAD TYPE	Itaipu Stabilizer Gain		
	$K_{pss} = 0$	$K_{pss} = 8$	$K_{pss} = 16$
Z	+ 0.656 ± j 5.38	− 0.114 ± j 5.33	− 0.333 ± j 5.21
I	+ 0.854 ± j 5.25	− 0.026 ± j 5.01	− 0.373 ± j 4.86
P	+ 1.05 ± j 5.10	+ 0.081 ± j 4.61	− 0.518 ± j 3.78

Table 3. Critical Eigenvalue as Affected by Load Type and Stabilizer Gain. Notation: Z = const. impedance, I = const. current and P = const. power.

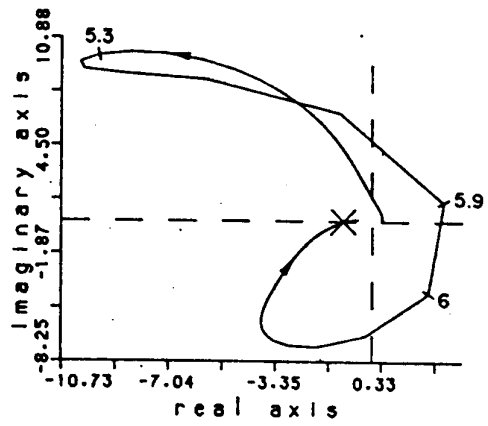

Figure 19.a. Polar Plot of $\Delta\omega(s)/\Delta V_r(s)$ for the Itaipu Generator

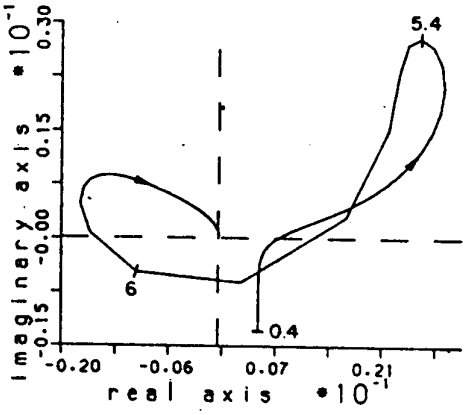

Figure 19.b. Polar Plot of $\Delta P_t(s)/\Delta V_r(s)$ for the Itaipu Generator

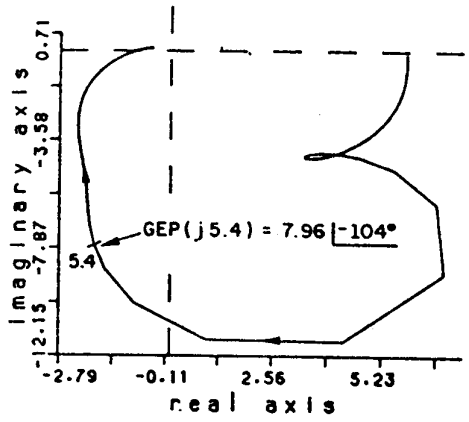

Figure 20.a. Polar Plot of GEP(s) for the Itaipu Generator

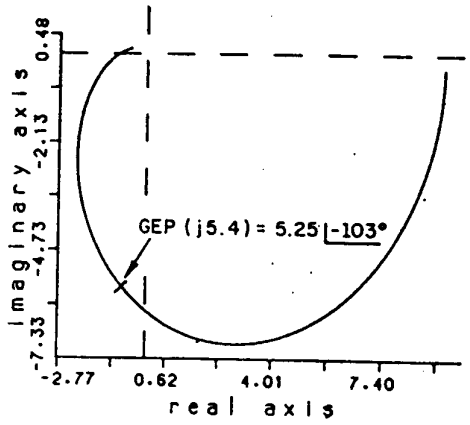

Figure 20.b. Polar Plot of GEP(s) for the Itaipu Generator with other machines represented as Infinite Buses

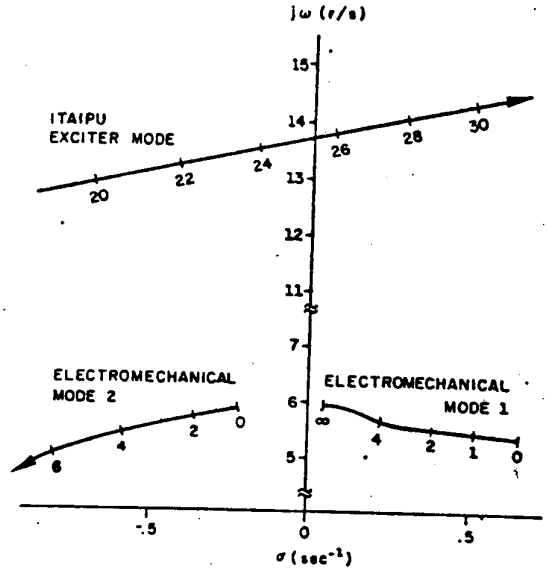

Figure 21 – Root Locus for $PSS_7(s)$ Stabilizer at Itaipu

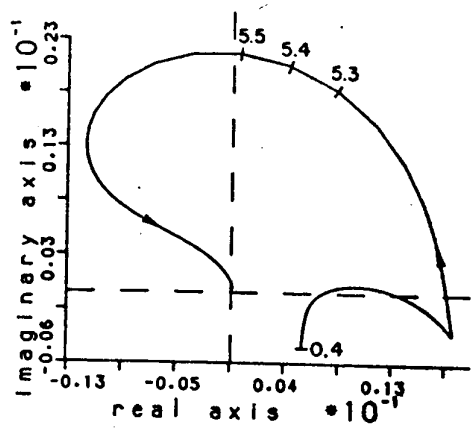

Figure 22.a. Plot of $\Delta\omega(s)/\Delta V_r(s)$ for the Itaipu Generator (3 Generators with PSS)

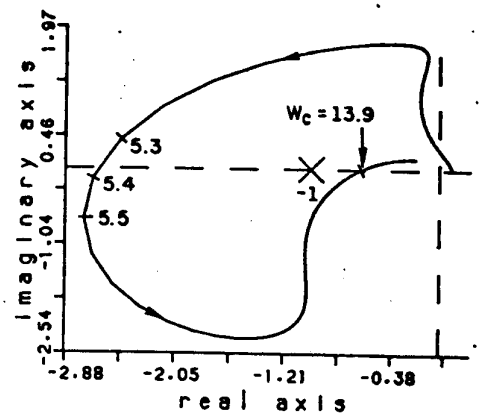

Figure 22.b. Plot of $\Delta V_{pss}(s)/\Delta V_r(s)$ for the $PSS_7(s)$ Stabilizer at Itaipu (3 gen. with PSS)

Figure 23.
Itaipu Power Deviations Following Pulse on the AVR reference.

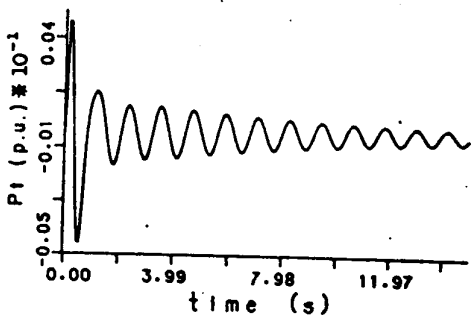

a.$PSS_7(s)$ has $K_{pss} = 8$ with Constant Z Loads

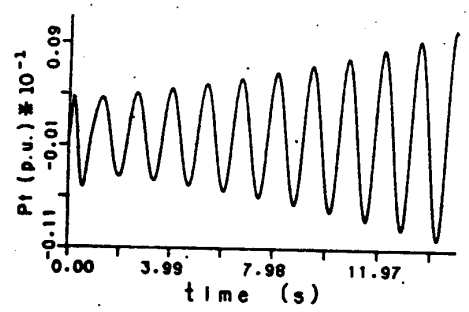

b. $K_{pss} = 8$ with Constant P Loads

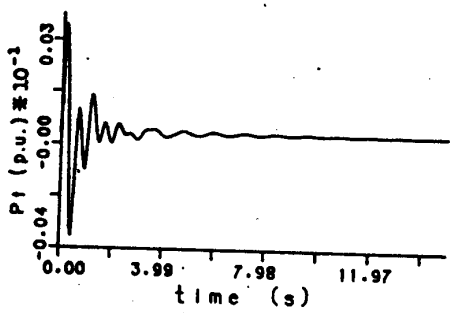

c. $K_{pss} = 16$ with Constant Z Loads

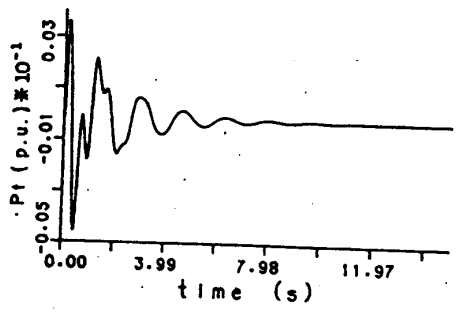

d. $K_{pss} = 16$ with Constant P Loads

7. FINAL COMMENTS

This paper dealt with small–signal stability problems associated with electromechanical oscillations in power systems. Phenomena such as subsynchronous resonance which require the representation of generator stator and network dynamics were considered out of the scope of this paper.

It was seen that the design of stabilizing signals to be added to generator AVR's, static VAr compensators or HVDC links can be carried out using similar transfer function block diagrams and the same frequency response technique. Eigenvalue analysis is needed to obtain information on open–loop and closed–loop system stability. The results presented in this paper, regarding the generator stabilizer (PSS), show some of the advantages of the accelerating power signal over the others and also show that bus terminal frequency leads to reduced gain margins when compared to the rotor speed signal. The frequency of the synthetic voltage E_q, on the other hand, has a performance equivalent to that of the rotor speed signal. The exercise with System I was also meant to show that almost any measurable system variable may be used as input to a stabilizer, which has the task of providing the right phase and gain compensation. It is obviously required that the undamped oscillatory mode be observable in the chosen input variable to the stabilizer.

Present day algorithms allow the efficient calculation of the dominant eigenvalues of large scale systems. The use of frequency response techniques for large–scale power systems remains computationally expensive despite the full exploitation of the Jacobian matrix sparsity. Large improvements can be obtained, when performing repeated studies, by calculating external system equivalents for discrete values of frequencies within the range of interest and storing them on magnetic disk for future use. Repeated frequency response studies can afterwards be done on the internal system, considering the full system dynamics, at the cost of solving only the internal system [10].

The possibility of obtaining frequency response between any two variables on a system is highly important for providing directly the compensation requirements of a control loop, be it an AVR, static compensator or HVDC link. These frequency responses are obtained for the plant in a multimachine context without the necessity of employing system simplification or reduced order equivalents.

Transfer function residues, controllability and observability factors are very useful in identifying best locations for placing stabilizing signals and best variables to be fedback through these signals. They can be obtained in a fraction of the time needed to calculate a single eigenvalue using present day algorithms for large scale systems [2].

The control difficulties which occur with the Itaipu generator in System II are due to improperly located zeros, and disappear when stabilizers are added to other generators in the system. This facts suggests that it may be good practice to have a high redundancy in stabilizing action, provided the generator stabilizers have moderate gains. The detrimental interaction between stabilizers in different power stations is not judged to be a problem at present.

With the exception of the P–Q plots of Section 5, this paper results are restricted to a single operating point of the two systems analyzed. Note that linear analysis tools should be used with the necessary care due to the non–linear nature of power systems. Many operating conditions should be analyzed with these linear tools and transient stability programs to ensure adequate stability margins at all cases.

We conclude by stressing the high benefits of having a comprehensive linear analysis package for the study of small–signal electromechanical stability problems. A good package should allow the study of large power systems, having a wide variety of components and controller structures, in a CAE environment, where various linear control methods can be used in a complementary manner.

ACKNOWLEDGEMENTS

The authors are indebted to Dr. F.M. Hughes, from UMIST, Manchester, England and Dr. J.C. Castro, from the Federal University of Paraíba, Brazil for their helpful suggestions. Numerous discussions with Prof. A.S. Pedroso and Mr. R. Baitelli, both from CEPEL, have been valuable in developing this work.

REFERENCES

[1] V. Arcidiacono, E. Ferrari, R. Marconato, J. Dos Ghali, D. Grandez, "Evaluation and Improvement of Electromechanical Oscillation Damping by Means of Eigenvalue–Eigenvector Analysis. Practical Results in the

Central Peru Power System" IEEE Trans. on Power Apparatus and Systems, Vol. PAS-99, pp. 769-778. March/April 1980.

[2] N. Martins, L.T.G. Lima, "Determination of Suitable Locations for Power System Stabilizers and Static VAr Compensators for Damping Electromechanical Oscillations in Large Scale Power Systems", Proc. of 1989 Power Industry Computer Application Conference, pp. 74-82, May 1989.

[3] N. Martins, "Efficient Eigenvalue and Frequency Response Methods Applied to Power System Small-Signal Stability Studies", IEEE Trans. on Power Systems, Vol. PWRS-1, pp. 217-226, February 1986.

[4] D.Y. Wong, G.J. Rogers, B. Porretta, P. Kundur, "Eigenvalue Analysis of Very Large Power Systems", IEEE Trans. on Power Systems, Vol. PWRS-3, pp. 472-480, May 1988.

[5] A. Semlyen, L. Wang, "Sequential Computation of the Complete Eigensystem for the Study Zone in Small Signal Stability Analysis of Large Power Systems". IEEE Trans. on Power Systems, Vol. PWRS-3, pp. 715-725, May 1988.

[6] N. Uchida, T. Nagao, "A New Eigen-Analysis Method of Steady-State Stability Studies for Large Power Systems: S Matrix Method". IEEE Trans. on Power Systems, Vol. PWRS-3, pp. 706-714, May 1988.

[7] L. Wang, A. Semlyen, "Application of Sparse Eigenvalue Techniques to the Small Signal Stability Analysis of Large Power Systems", Proc. of 1989 Power Industry Computer Application Conference, pp. 358-365, May 1989.

[8] G.J. Rogers, "Methods for Small Signal Analysis of Very Large Power Systems", Proc. of the 26th Conference on Decision and Control, Los Angeles, pp. 393-398, December 1987.

[9] F.L. Pagola, I.J. Pérez-Arriaga, G.C. Verghese, "On Sensitivities, Residues and Participations. Applications to Oscillatory Stability Analysis and Control". 1988 IEEE Summer Meeting, paper 88 SM 692-6.

[10] N. Martins, L.T.G. Lima, "Decomposition Technique for Efficient Computation of Small-Signal Stability Problems in Large Power Systems", Proc. of IASTED Conference on High Technology in the Power Industry, pp. 232-237, Scottsdale, Arizona, March 1988.

[11] K.E. Bollinger and others, "Power System Stabilization Via Excitation Control". IEEE Publication 81EH0175-0 PWR, 1981.

[12] F.M. Hughes, A.M.A. Hamdan, "Design of Turboalternator Excitation Controllers Using Multivariable Frequency - Response Methods", Proc. IEE, Vol. 123, No. 9, pp. 901-905, September 1976.

[13] E.V. Larsen, J.H. Chow, "SVC Control Design Concepts for System Dynamic Performance", in IEEE Tutorial Course: Application of SVS for System Dynamic Performance, 87 TH0187-5-PWR, pp. 36-53, 1987.

[14] P.Kundur, D.C. Lee, H.M. Zein El-Din, "Power System Stabilizers for Thermal Units: Analytical Techniques and on-site Validation", IEEE Trans. on PAS, Vol. PAS-100, pp. 81-95, January 1981.

[15] P. Kundur, M. Klein, G.J. Rogers, M.S. Zywno, "Application of Power System Stabilizers for Enhancement of Overall System Stability". IEEE Trans. on Power Systems, Vol. 4, No. 2, pp. 614-626, May 1989.

[16] J.F. Hauer, "Reactive Power Control as a Means for Enhanced Interarea Damping in the Western U.S. Power System - A Frequency-Domain Perspective Considering Robustness Needs", in IEEE Symposium on Application of SVS for System Dynamic Performance, Publication 87 TH0187-5-PWR, pp. 79-82, 1987.

[17] F.P. de Mello, L.N. Hannett, J.M. Undrill, "Practical Approaches to Supplementary Stabilizing from Accelerating Power", IEEE Trans. on PAS, Vol. PAS-97, pp. 1515-1522, 1978.

[18] D.N. Ewart, F.P. de Mello, "A Digital Computer Program for the Automatic Determination of Dynamic Stability Limits", IEEE Trans. on Power App. Systems, Vol. PAS-86, pp.867-875, 1967.

[19] A.M.A. Hamdan, "Vector Frequency Response Methods Applied to Turbo-Alternator Control", Ph.D Thesis, UMIST, Manchester, UK, 1976.

[20] J.M. Undrill, J.A. Casazza, E.M. Gulachenski and L.K. Kirchmayer, "Electromechanical Equivalents for Use in Power System Stability Studies", IEEE Trans. on Power App. Systems, pp. 2060-2071, Sept/Oct. 1971.

Appendix 1. Complete Data for System I

Frequency = 60Hz; MVA base = 300

Bus Data

Bus nº	Voltage Magnitude (pu)	Voltage Angle (degrees)	Generation MW	Generation MVAr
1	1.	49.8	250	61.5
2	.989	24.9		
3	1.	0.	-250	61.5
4	.989	24.9		

The shunt capacitor at bus 2 has an admittance of 0 + j 0.333 p.u.

Line Data

From	To	R + jX(pu)
1	2	0.+ j 0.5
2	3	0.+ j 0.5
2	4	0.+ j 0.3

Synchronous Generator Data

MVA base	=	300			
T'_{do}	=	8.5 s	X''_d	= 0.26	pu
T''_{do}	=	0.03 s	T''_{qo}	= 0.90 s	
R_a	=	0.0	X''_q	= 0.26 pu	
X_d	=	2.72 pu	X_q	= 2.6 pu	
X'_d	=	0.36 pu	H	= 3.84 kWs/kVA	

System Controllers

The automatic voltage regulator has the following transfer function:

$$AVR(s) = 50/(1 + s0.05)$$

The static compensator controls the voltage magnitude of bus 4 and has, at the system MVA base, the following transfer function:

$$SVC(s) = \left(\frac{800}{1 + s0.05}\right)\left(\frac{1 + s}{1 + s5}\right)^2$$

The power system stabilizers sensitive to the generator rotor speed deviations have the transfer functions:

$$PSS_1(s) = 7\left(\frac{s3}{1 + s3}\right)\left(\frac{1 + s0.3}{1 + s0.075}\right)^2$$

$$PSS_2(s) = -116\left(\frac{s3}{1 + s3}\right)\left(\frac{1 + s0.05}{1 + s0.45}\right)^2$$

The power system stabilizer sensitive to terminal power deviations has the transfer function:

$$PSS_3(s) = -0.7\left(\frac{s3}{1 + s3}\right)\left(\frac{1 + s0.14}{1 + s0.28}\right)$$

Bus frequency deviations are simulated by passing the phase angle signal, whose exact expression is easily obtained, through a derivative block having a small time constant (1 ms in this paper). This extra block is added to the stabilizing signal transfer function.

The power stabilizer sensitive to per unit terminal bus frequency has the transfer function:

$$PSS_4(s) = 10.5\left(\frac{s3}{1 + s3}\right)\left(\frac{1 + s0.3}{1 + s0.075}\right)^2\left(\frac{s}{1 + s0.001}\right)$$

The power system stabilizer sensitive to deviations in the apparent resistance of the line between buses 1 and 2 has the function:

$$PSS_5(s) = 1.4\left(\frac{s3}{1 + s3}\right)\left(\frac{1 + s0.14}{1 + s0.56}\right)$$

The static compensator stabilizing signal, when sensitive to the per unit frequency deviations of bus 2 has the following transfer function:

$$CSS_1(s) = 148\left(\frac{s3}{1 + s3}\right)\left(\frac{1 + s0.14}{1 + s0.28}\right)\left(\frac{s}{1 + s0.001}\right)$$

For a compensator stabilizer sensitive to transit power deviations in the line between buses 2 and 3, two transfer functions are considered:

$$CSS_2(s) = 0.1522\left(\frac{s3}{1 + s3}\right)\left(\frac{1 + s0.3}{1 + s0.075}\right)^2$$

$$CSS_3(s) = 0.12\left(\frac{s3}{1 + s3}\right)\left(\frac{1 + s0.6}{1 + s0.1}\right)^2\left(\frac{1 + s0.02}{1 + s0.1}\right)^2$$

Generator Model

The fifth-order model for the synchronous generator is described by the following equations:

$$\frac{d}{dt}(E_q') = \frac{1}{T_{do}'}(E_{fd} - (X_d - X_d')I_d - E_q')$$

$$\frac{d}{dt}(E_d'') = \frac{1}{T_{qo}''}((X_q - X_q'')I_q - E_d'')$$

$$\frac{d}{dt}(E_q'') = \frac{1}{T_{do}''}(E_q' - (X_d' - X_d'')I_d - E_q'')$$

$$\frac{d}{dt}(\omega) = \frac{1}{2H}(P_m - P_e)$$

$$\frac{d\delta}{dt} = \omega_0(\omega - 1)$$

The generator algebraic equations are:

$$E_d'' - V_d = R_a I_d - X_q'' I_q$$

$$E_q'' - V_q = X_d'' I_d + R_a I_q$$

Terminal voltage and electrical power are given by:

$$V_t^2 = V_d^2 + V_q^2$$

$$P_e = V_d I_d + V_q I_q$$

Appendix 2. Complete Data for Study System II

Frequency = 60 Hz; MVA base = 1000

Bus Data

Bus	Voltage Magnitude	Voltage Angle	Generation MW	Generation MVAr
1	1.03	24.5°	1658.	−412.0
2	1.03	27.2°	1332.	−200.1
3	1.029	26.6°	1540.	−446.5
4	1.039	48.5°	6500.	1958.6
5	.998	21.2°		
6	.989	21.4°		
7	0.966	0.	−3164.	952.7

Bus	Load MW	Load MVAr	Shunt (p.u)
1	2405.	−467.	0.1792
2	692.3	−184.	0.1491
3	688.2	−235.	0.1142
4	62.6	24.3	0.0368
5	845.8	−9.2	0.0330
6	−4.9	79.8	2.1420
7	2884.	−196.	0.0420

Line Data

From	To	R + j X (pu)
1	3	0.003 + j 0.038
2	3	0.005 + j 0.076
4	6	0.0029 + j 0.0731
5	1	0.019 + j 0.215
5	2	0.015 + j 0.225
6	5	0 + j 0.039
6	7	0.004 + j 0.057

The line susceptances of this 7-bus equivalent were combined with the bus shunt reactors, and the total values are given in the bus data.

Synchronous Generator Data

	GENERATOR BUS				
	1	2	3	4	7
MVA	1900	1400	1944	6633	6000
T'_{do}	5.	5.	5.	7.6	8.
T''_{do}	.053	.053	0.06	0.09	0.09
T''_{qo}	.123	.123	0.09	0.19	0.2
H	4.5	4.5	4.5	5.07	5.
X_d	0.85	0.85	0.88	0.9	1.
X_q	0.7	0.7	0.69	0.68	0.7
X'_d	0.3	0.3	0.3	0.3	0.3
X''_d	0.2	0.2	0.2	0.24	0.25
X''_q	0.2	0.2	0.2	0.27	0.25

The stator resistances and mechanical damping constants D are zero for all machines. All five machines have the same first-order model and parameters for the excitation control system: AVR(s) = 30/(1 + s 0.05). Prime movers and speed-governor effects are not represented. All power system stabilizers considered in this study are sensitive to rotor speed deviations.

The power system stabilizers added to the generators located at buses 1, 2 and 3 have the same transfer function:

$$PSS_6(s) = 10 \frac{s3}{1 + s3} \left(\frac{1 + s0.3}{1 + s0.075}\right)^2$$

The root locus plot of Figure were made considering the following stabilizer at the Itaipu generator:

$$PSS_7(s) = K_{pss} \left(\frac{s3}{1 + s3}\right) \left(\frac{1 + s0.52}{1 + s0.065}\right)^2$$

The polar plot and eigenvalue results presented for System II were obtained with K_{pss}=16 for the Itaipu stabilizer.

Appendix 3. Power System Data Used for Obtaining P–Q Curves

The network, generator and induction motor parameters are all given on a 500 MVA base.

The voltage at bus 1 is held at 1 p.u. and the load of bus 2 is held approximately constant at $P_L + j\,Q_L = 504 + j\,279$.

The generator parameters are the same as those of System I. The automatic voltage regulator and rotor speed derived stabilizer have transfer functions:

$$AVR(s) = 40/(1 + s0.05)$$

$$PSS(s) = 2 \left(\frac{s3}{1 + s3}\right) \left(\frac{1 + s0.3}{1 + s0.075}\right)^2$$

The induction motor data are

R_a = 0.00667

R_r = 0.0143

X_0 = 2.9

X' = 0.193

T'_0 = 0.599

H = 0.5 or 5 seconds.

Appendix 4.Polar Plots of Input Signals of System I Used in Stabilizer Design

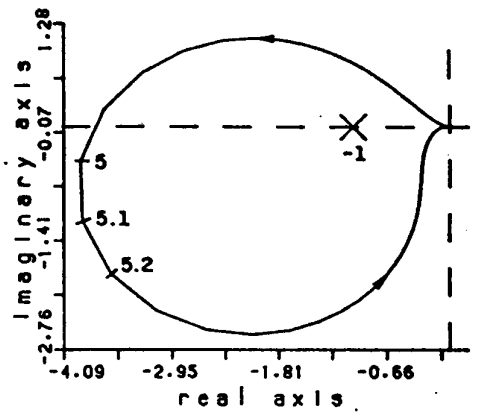

Figure A4.1. Polar Plot of $\Delta P_t(s)/\Delta V_r(s)$

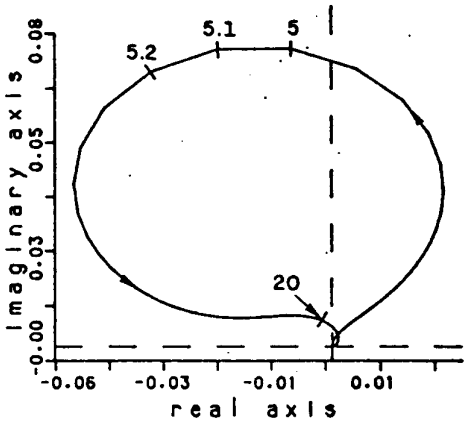

Figure A4.2. Polar Plot of $\Delta \theta_1(s)/\Delta V_r(s)$

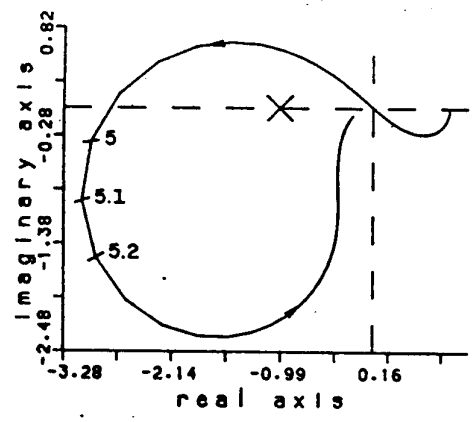

Figure A4.3. Polar Plot of $\Delta R(s)/\Delta V_r(s)$

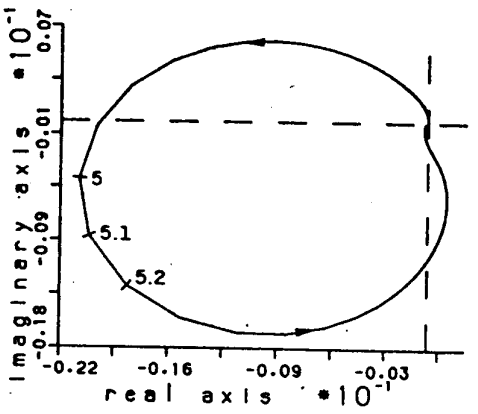

Figure A4.4. Polar Plot of $\Delta\theta_2(s)/\Delta V_{rc}(s)$

Appendix 5. Redundancy in the Rotor Swing State Variables

The automatic formation of the system matrices is carried out in terms of the absolute deviations of the rotor speed and angle state variables. As a consequence, the state matrix of a power system without an infinite–bus will show either one or two zero eigenvalues. One appears as a result of the redundancy in rotor angle state variables, since the state of the system is defined by the relative angular positions of the generator rotors, rather than by their absolute values.

The other zero eigenvalue appears if turbo–generator torques are all assumed independent of speed deviations. This zero eigenvalue will not exist if a damping term is included in the rotor motion equation of a single generator of the system or if speed–governors are modelled.

The redundancy in rotor angular position states can be eliminated by choosing the relative angular positions as the new states.

$$p\,\Delta\delta_r = 0$$

$$p\,\Delta\delta_{jr} = \omega_o\,\Delta\omega_j - \omega_o\Delta\omega_r \qquad \text{(A5.1)}$$

for $j \in (1,2,\ldots, r-1, r+1,\ldots, ng)$, r being the reference generator.

The second zero eigenvalue, if present, can also be eliminated by choosing relative speed deviations rather than absolute ones as the state variables.

$$p\,\Delta\omega_r = 0$$

$$p\,\Delta\omega_{jr} = -\frac{1}{2\,H_j}\,\Delta P_{ej} + \frac{1}{2\,H_r}\,\Delta P_{er} \qquad \text{(A5.2)}$$

The procedures described is equations (A5.1) and (A5.2) are actually similarity transformations [19]. The choice of one or another machine as the angular reference is done by performing different matrix similarity transformations. Similar matrices have the same eigenvalues, and therefore the choice of one or another generator as the angular reference (or even having no angular reference) should theoretically be of no consequence to the results.

The power system state matrix has a mixture of well–conditioned and ill–conditioned eigenvalues. The two zero eigenvalues are ill–conditioned and highly dependent on the exactness of the network solution (the state matrix is singular only if the network solution is exact). Normal power flow mismatch errors cause these eigenvalues to assume small values around the origin, and in most instances one of them has a positive real part. It was a wrong interpretation of this fact that led some researchers [20] to believe that correct results could only be obtained if a specific generator in the system was chosen as the angular reference.

It is always recommended to perform the similarity transformation of equation (A5.1) so as to eliminate this unwanted and ill–conditioned root. Expressing the equations in terms of relative generator rotor speeds (equation A5.2) is however not needed in our analysis.

Nelson Martins (M'1981) received his B.Sc. degree from the University of Brasilia, Brazil, in 1972. He received the M.Sc. and Ph.D. degrees, both in electrical engineering, from the University of Manchester, UK, in 1974 and 1978 respectively.

Dr.Martins is presently a senior research engineer at CEPEL, the Brazilian electrical energy research center located in Rio de Janeiro. He developed new digital–computer tools and authored many papers in the area of power system dynamics and control.

Leonardo T.G. Lima received his B.Sc. degree in electrical engineering from the Federal University of Rio de Janeiro, Brazil, in 1986.

Mr.Lima worked in CEPEL until September 1988 when he joined MAIN Engenharia S.A., an electrical consultant firm in Rio de Janeiro. His current work and interests include power system dynamics and development of large scale power system analysis tools.